Journal of Alloys and Compounds 782 (2019) 1076–1086

Contents lists available at ScienceDirect

Journal of Alloys and Compounds

journal homepage: http://www.elsevier.com/locate/jalcom

Improvement of mechanical properties and reduction of yield asymmetry of extruded Mg-Sn-Zn alloy through Ca addition

Yanfu Chai [a], Bin Jiang [a, b, *], Jiangfeng Song [a, **], Qinghang Wang [a], Hang Gao [a], Bo Liu [c], Guangsheng Huang [a], Dingfei Zhang [a], Fusheng Pan [a, b]

[a] State Key Laboratory of Mechanical Transmissions, College of Materials Science and Engineering, Chongqing University, Chongqing, 400044, China
[b] Chongqing Academy of Science and Technology, Chongqing, 401123, China
[c] Chongqing Chang-an Automobile Co., Ltd., Chongqing, 400023, China

ARTICLE INFO

Article history:
Received 13 November 2018
Received in revised form
6 December 2018
Accepted 7 December 2018
Available online 8 December 2018

Keywords:
Mg-1.0Sn-0.5Zn alloy
Ca content
Microstructure
Texture
Mechanical properties

ABSTRACT

Effects of Ca content (0.0, 0.5, 1.0, 2.0 wt%) on the microstructure, texture and mechanical properties of Mg-1.0Sn-0.5Zn-based alloys were investigated. The results stated that secondary phase of Mg-Sn-Zn alloy was transformed from Mg_2Sn to CaMgSn and Mg_2Ca with an increase in the Ca content. Ca addition also seriously affected the dynamic recrystallization and texture formation during the extrusion process. As for the as-extruded alloys, as Ca content increased from 0.0 to 2.0 wt%, the grain size was significantly decreased from ~25 μm to 4–6 μm, whereas the texture type was converted from strong basal texture into weakened extrusion direction (ED)-split texture. Under tension, the elongation to fracture of the as-extruded Mg-Sn-Zn alloy was increased initially with the addition of Ca (0.0–1.0 wt%), and then decreased after 2.0 wt% Ca addition, whereas the counterpart in compression was changeless regardless of Ca content. Both tensile and compressive yield strengths of Mg-Sn-Zn alloy were monotonously increased with increasing Ca content, whereas this increment of yield strength induced by Ca addition was more pronounced in compression than that in tension. Obviously improved tension-compression yield asymmetry of Mg-Sn-Zn alloy via Ca addition was ascribed to grain refinement, texture modification and newly formed CaMgSn and Mg_2Ca phase precipitates.

1. Introduction

Magnesium (Mg) alloys with low density, high strength-to-weight ratio and good castability were commonly used in automotive, aircraft, aerospace and consumption electrical products [1–3]. However, undesirable strength and ductility of Mg alloys severely limited their further industrial applications [4]. Alloying was recognized as an effective and promising method to enhance mechanical properties by influencing the grain size, precipitates and texture of magnesium alloys [5]. Among many alloy elements, Sn element with a low price, has received more and more attention for alloying with Mg alloys in recent years. Previous research [6] reported that the addition of Sn to pure Mg can remarkably reduce the critical resolved shear stress (CRSS) of pyramidal slip and consequently contribute to formability improvement. Zhao et al. [7] also concluded that tensile strength and ductility of as-extruded Mg alloys can be simultaneously improved as Sn content increases from 1.3 to 4.7 wt%. Another alloying element that has been conventionally applied in Mg alloys is Zn. Zn element plays a crucial role in solid solution strengthening and precipitation hardening [8,9]. For Mg-Sn alloy system, the addition of Zn could enhance its aging hardening responses and mechanical properties due to the more uniformly dispersed and finer Mg_2Sn precipitates [10–12]. Hence, Mg-Sn-Zn based alloys appear to be promising for the development of high-performance Mg alloys.

In order to promote the further popularization and application of Mg-Sn-Zn alloy system, micro-alloying by adding other elements is very necessary. Ca element with abundant reserves was capable of reducing flammability [13], refining grains [14] and modifying texture [15] of Mg alloys. Pan et al. [16] found that Ca and/or Zn

* Corresponding author. State Key Laboratory of Mechanical Transmissions, College of Materials Science and Engineering, Chongqing University, Chongqing, 400044, China.
** Corresponding author.State Key Laboratory of Mechanical Transmissions, College of Materials Science and Engineering, Chongqing University, Chongqing, 400044, China.
E-mail address: jiangbinrong@cqu.edu.cn (B. Jiang).

https://doi.org/10.1016/j.jallcom.2018.12.109
0925-8388/

addition can simultaneously enhance the strength and ductility of Mg-2wt.% Sn alloy. Besides, they also developed a novel low-alloyed Mg-2Sn-2Ca alloy (in wt.%) that exhibited ultra-high tensile yield strength (360–440 MPa) after indirect extrusion at the 220–320 °C [17]. However, to the authors' knowledge, no detailed research has been conducted on the accurate effect of Ca content on microstructure, texture and mechanical performance of Mg-Sn-Zn alloy containing low Sn content.

Thus, in the present study, the effects of Ca content on dynamic recrystallization and texture formation of Mg-Sn-Zn alloy during the extrusion process were disclosed. Moreover, the mechanical properties and tension-compression yield asymmetry of as-extruded Mg-1.0Sn-0.5Zn-*x*Ca ($x = 0.0$, 0.5, 1.0, 2.0 wt%) alloys were primarily studied. Such an investigation will provide an important basis for enhancing the mechanical properties of Mg-Sn-Zn alloys, which may promote their practical applications.

2. Experimental procedure

In argon atmosphere, pure Mg ingots with 1.0 wt% Sn, 0.5 wt% Zn and various content of Ca (0.0, 0.5, 1.0 and 2.0 wt%) were melted at 720 °C in a graphite mold using an induction furnace and then poured into a cylindrical shaped steel mold cavity preheated to 300 °C. The chemical compositions of the cast billets were subsequently confirmed by X-ray fluorescence spectrometer (XRF-1800CCDE) and corresponding results were listed in Table 1. Cast billets were homogenized (380 °C for 12 h under the atmosphere of argon gas) and then extruded at 360 °C with an extrusion ratio of 32:1 to obtain a sheet of 56 mm in width and 3 mm in thickness. Microstructural characteristics were analyzed by optical microscopy (OM), scanning electron microscope (SEM), energy dispersive X-ray spectroscopy (EDS), X-ray diffraction (XRD), electron backscatter diffraction (EBSD) and transmission electron microscopy (TEM). OM (ZEISS, Axiovert 40 MAT) and SEM (Tescan Vega 3 LMH) observations were prepared following a standard procedure of grinding, polishing and etching (5 g picric acid + 5 ml acetic acid + 10 ml water + 100 ml ethanol). The average grain size was measured by using the standard linear-intercept method. The volume fraction of secondary phase particles was evaluated by using Image-Pro Plus software, and the results were determined by averaging the values taken from at least five separate SEM images. XRD measurements were conducted on an X-ray diffractometer (Rigaku D/MAX-2500PC) to further identify the formed precipitated particles. Sample preparations for EBSD observation were consisted of mechanical grounding and electrochemical polishing in an AC2 electrolyte through application of a voltage of 20 V for ~70 s at −20 °C. The EBSD data were collected using a JEOL JSM-7800F scanning electron microscope operating at 20 kV with a step size of 0.8 μm and then analyzed with orientation imaging microscopy (OIM, HKL-channel 5) software. Thin foil specimens for TEM (FEI TECNAI G2 F20) observation were prepared through mechanical polishing and ion-beam thinning using a Gatan Precision Ion Polishing System at room temperature.

Uniaxial tensile and compressive tests were both carried out on a CMT6305-300 KN testing machine using an initial strain rate of $10^{-3}\ S^{-1}$ at room temperature. Both tensile specimens with dimension of 14 mm gauge length × 6 mm gauge width × 3 mm gauge thickness and compressive specimens with dimension of 10 mm gauge length × 8 mm gauge width × 3 mm gauge thickness were machined from the as-extruded sheets along extrusion direction (ED). Three samples were conducted in each group to warrant the experimental precision. The 0.2% proof stress ($\sigma_{0.2}$) was deemed to the yield strength (YS) and the ratio of the YS in compression to the YS in tension was denoted as asymmetry ratio (CYS/TYS) here.

Table 1
Chemical compositions of the as-cast Mg-1.0Sn-0.5Zn-based alloys.

Designation	Nominal alloy	Composition (wt.%)			
		Sn	Zn	Ca	Mg
Alloy I	Mg-1.0Sn-0.5Zn-0.0Ca	1.16	0.48	–	Bal.
Alloy II	Mg-1.0Sn-0.5Zn-0.5Ca	1.10	0.55	0.54	Bal.
Alloy III	Mg-1.0Sn-0.5Zn-1.0Ca	0.98	0.54	1.05	Bal.
Alloy IV	Mg-1.0Sn-0.5Zn-2.0Ca	1.01	0.57	2.26	Bal.

3. Results

3.1. Microstructure characterization

Fig. 1 shows the OM and backscattered electron (BSE) SEM images of as-cast Mg-1.0Sn-0.5Zn-*x*Ca ($x = 0.0$, 0.5, 1.0, 2.0 wt%) alloys. It is evident that Mg-1.0Sn-0.5Zn ternary alloy exhibits a structure similar to equiaxed grains (see Fig. 1a), while Ca-modified samples all display typical α-Mg dendrites, and dendritic arm spacing (DAS) of the primary α-Mg can be obviously refined with increasing Ca content (see Fig. 1c, e, g). Combined XRD patterns (see Fig. 2) with SEM micrographs, it can be concluded that Mg-1.0Sn-0.5Zn alloy comprises primary α-Mg (dark colour), Sn-rich segregation (gray band) and few spherical Mg_2Sn phase (white tiny particles). With the increase of Ca addition, needle or sphere-like CaMgSn precipitates can be detected as discontinuous phases, which are mainly scattered along dendrite boundaries. This observation is in accordance with the research of Mahmudi et al. [18,19], which declared that Ca addition into Mg-5Sn (in wt.%) alloy facilitated the formation of a more thermally stable CaMgSn phase rather than Mg_2Sn phase. Moreover, the volume fraction of the secondary phase (white area) increases considerably with increasing of Ca content, especially the sphere Mg_2Ca [20] precipitates. Additionally, extra small diffraction peaks of $Ca_2Mg_6Zn_3$ [21] intermetallic phases can be also observed in the XRD patterns of Ca-modified samples. As a result, the addition of Ca to a ternary Mg-Sn-Zn alloy leads to changes in the secondary phase particles from Mg_2Sn to CaMgSn, Mg_2Ca and $Ca_2Mg_6Zn_3$ (in the minority).

Fig. 3 presents the OM images of the as-extruded Mg-1.0Sn-0.5Zn-based alloys on the ED-normal direction (ND) plane with different Ca content. Compared with as-cast alloys, the grain sizes of these as-extruded alloys are significantly refined due to the dynamic recrystallization (DRX) during the extrusion process. The measured average grain size of as-extruded Mg-1.0Sn-0.5Zn alloy is approximately 24.9 μm (geometric standard deviation, $\sigma = 3.2$), while for the Mg-Sn-Zn-Ca quaternary alloys, the corresponding values are significantly decreased to 5.8 μm ($\sigma = 1.1$), 5.4 μm ($\sigma = 1.2$) and 3.8 μm ($\sigma = 0.6$) as Ca addition from 0.5, 1.0 to 2.0 (in wt.%), separately. This indicates that grain size is significantly changed upon Ca addition, and a more pronounced grain refinement can be achieved with a higher Ca content. Moreover, it can be observed from the BSE SEM images (see Fig. 4) that the secondary phase particles are partially broken during the extrusion process and form strips with a white contrast along the ED, meanwhile the concentration of the strips increases with increasing Ca content. In order to further reveal the secondary phase particles in as-extruded Ca-modified samples, the corresponding EDS mapping images and details of typical precipitates of as-extruded Mg-1.0Sn-0.5Zn-2.0Ca alloy are shown in Fig. 5. It is observed that spherical Mg_2Ca particles (200–700 nm in diameter) are distributed in clusters, whereas the blocky CaMgSn particles (260 nm-1.25 μm in length; 160–980 nm in width) are relatively more dispersed. The above results coincides well with the observation results of as-cast

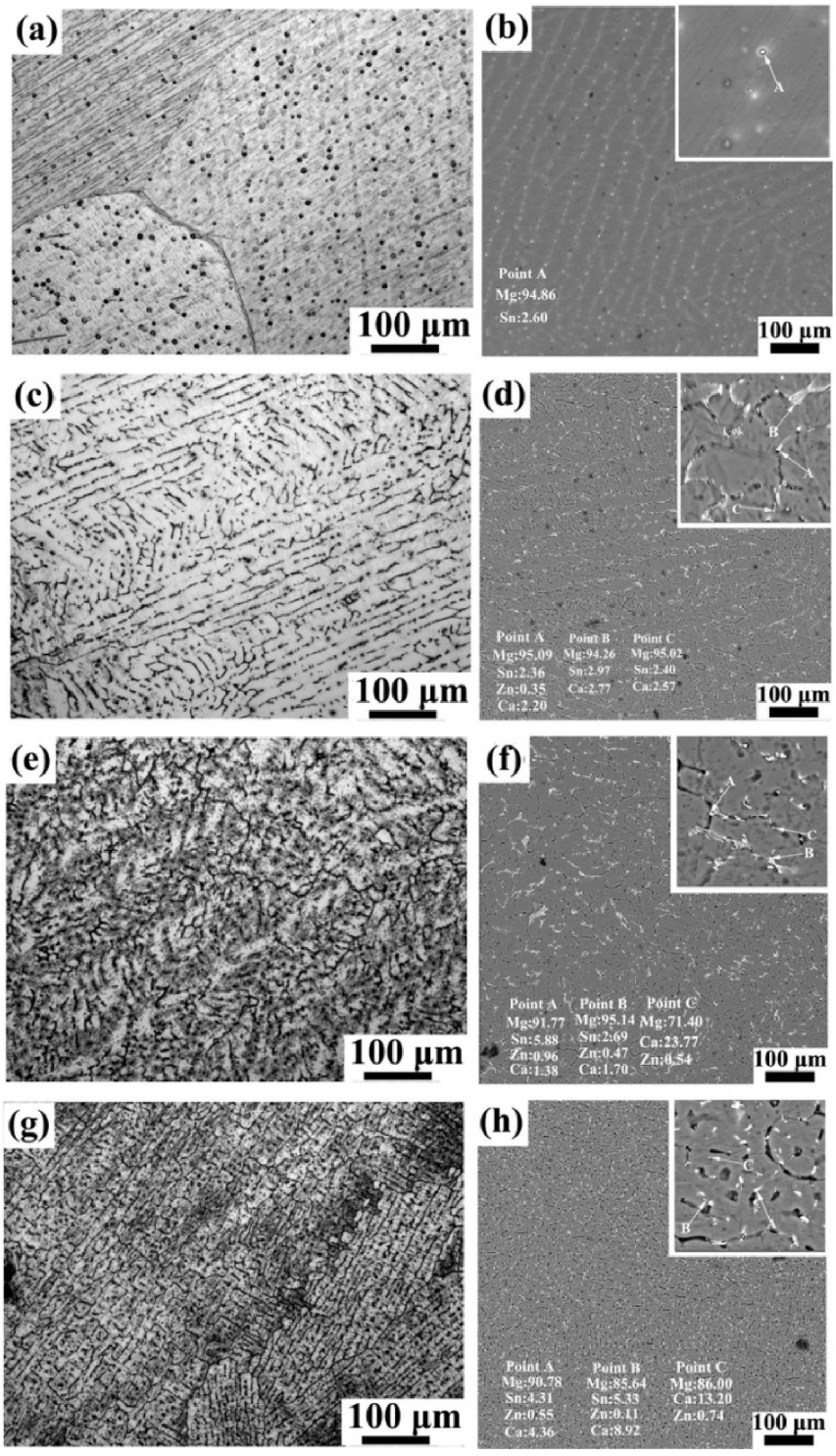

Fig. 1. OM and Backscattered electron (BSE) SEM images of the as-cast Mg-1.0Sn-0.5Zn-based alloys: (a) OM image and (b) BSE SEM image obtained from Mg-1.0Sn-0.5Zn alloy; (c) OM image and (d) BSE SEM image obtained from Mg-1.0Sn-0.5Zn-0.5Ca alloy; (e) OM image and (f) BSE SEM image obtained from Mg-1.0Sn-0.5Zn-1.0Ca alloy; (g) OM image and (h) BSE SEM image obtained from Mg-1.0Sn-0.5Zn-2.0Ca alloy.

samples, and further identification confirmed that CaMgSn and Mg_2Ca exist as the dominant secondary phases in Mg-Sn-Zn-Ca alloys.

Fig. 6 displays the representative EBSD inverse pole figure (IPF) maps and (0001) pole figures of as-extruded Mg-1.0Sn-0.5Zn-based alloys. Fig. 7(a) and (b) show the detailed distribution of texture intensity in the basal poles plane plotted as a function of tilt from the ND toward the ED or transverse direction (TD), respectively. There is obvious grain refinement and a weakened texture with splitting of their basal poles to the ED in Ca-modified samples, compared with Mg-1.0Sn-0.5Zn alloy with coarse grains and strong basal texture (slight spreading basal poles toward the TD due to Zn

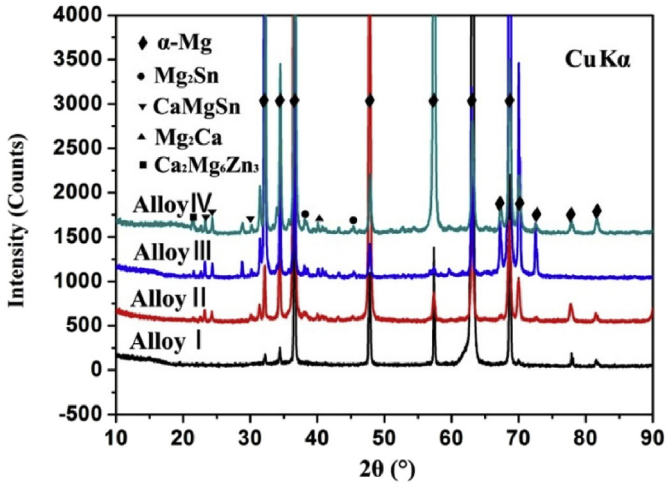

Fig. 2. XRD patterns of the as-cast Mg-1.0Sn-0.5Zn-*x*Ca series alloys.

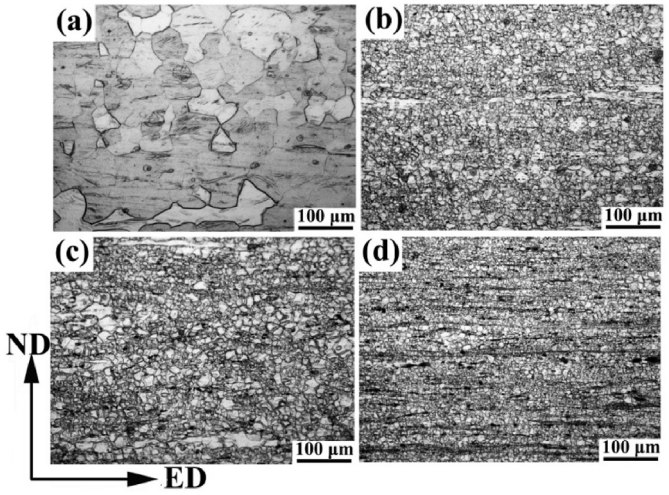

Fig. 3. Optical micrographs of as-extruded samples: (a) Mg-1.0Sn-0.5Zn alloy. (b) Mg-1.0Sn-0.5Zn-0.5Ca alloy. (c) Mg-1.0Sn-0.5Zn-1.0Ca alloy. (d) Mg-1.0Sn-0.5Zn-2.0Ca alloy.

addition [22]). Furthermore, this split degree becomes more severe with increasing the content of Ca. Therefore, it can be concluded that Ca addition is effective for grain refinement and texture modification of as-extruded Mg-Sn-Zn alloy.

3.2. Mechanical properties

Fig. 8 presents the true stress–true strain curves of the as-extruded Mg-1.0Sn-0.5Zn-based alloys from tension and compression tests. The mean values and standard deviations of the tensile and compressive properties are summarized in Table 2. Besides, the ratio between compressive and tensile yield strength (CYS/TYS) is also calculated. Under tension, tensile yield strength (TYS) continuously increases as the Ca content increases. Especially, the TYS of Mg-1.0Sn-0.5Zn-2.0Ca alloy reaches up to 180.7 MPa, enhanced by approximately 34% than that of Mg-1.0Sn-0.5Zn alloy. The ultimate tensile strength (UTS) and elongation to fracture (EL) both improved initially with the addition of Ca, and then decreased. The Mg-1.0Sn-0.5Zn-1.0Ca alloy possesses the highest values of UTS (310.9 MPa) and EL (23.8%) among Mg-1.0Sn-0.5Zn-based alloys, which increased by about 50 MPa and 6.4% than those of Mg-1.0Sn-0.5Zn alloy, respectively. Under compression, both compressive yield strength (CYS) and ultimate compressive strength (UCS) increase as the Ca addition. Especially, the CYS and UCS of the Mg-1.0Sn-0.5Zn-2.0Ca alloy are as high as 151.1 and 339.9 MPa, respectively, about 96.6 MPa and 29.4 MPa higher than those of the Mg-1.0Sn-0.5Zn alloy. Besides, EL values are similar in the range of 16–19% despite the different content of Ca, which implies that compressive ductility is not sensitive to the Ca content. Additionally, it is quite obvious that the increment of the CYS resulting from Ca addition appears to be much greater than that of TYS does. Hence, compared with the Mg-1.0Sn-0.5Zn alloy (0.40), the CYS/TYS ratios are dramatically increased to 0.72, 0.79 and 0.84 as Ca addition changed from 0.5, 1.0 to 2.0 (in wt.%). This indicates that the tension-compression yield asymmetry of as-extruded Mg-Sn-Zn alloy decreases significantly with the addition of Ca.

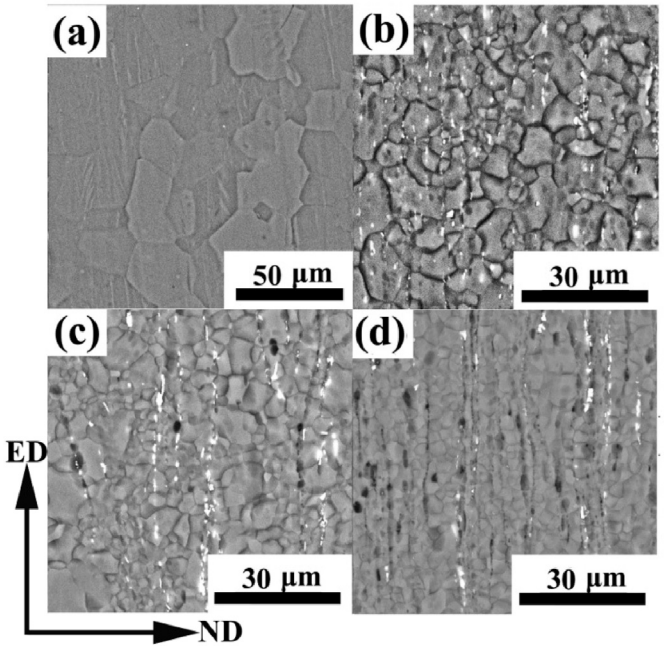

Fig. 4. The backscatter SEM images of as-extruded Mg-1.0Sn-0.5Zn-*x*Ca alloys: (a) 0.0 Ca alloy; (b) 0.5 Ca alloy; (c) 1.0 Ca alloy; (d) 2.0 Ca alloy.

4. Discussion

4.1. The microstructure variation with Ca addition

4.1.1. Grain size

As showed in Fig. 1, for the as-cast Mg-Sn-Zn alloy, Ca addition results in grain refinement and microstructure modification from equiaxed-liked grains to typical dendrites. Meanwhile, more refined DAS can be achieved with further Ca content increases. This derives from the solute segregation [23] and the restriction imposed by intermetallic compounds that were densely distributed along grain boundaries [24]. It is generally accepted that Ca element possesses a high growth restriction factor (11.47) and slow diffusion rate [25]. Hence, the enrichment of Ca atoms in front of the liquid/solid interface can bring out intensive constitutional undercooling, which ultimately prevent grains from growing up and in favor of dendrite's formation [26]. Besides, the emergence of thermally stable CaMgSn and Mg_2Ca phase particles may accelerate nucleation rate, enhance pinning grain boundary ability, and consequently restrict dendrite growth (i.e. decrease of the DAS).

As seen in Fig. 3, the addition of Ca can produce the powerful

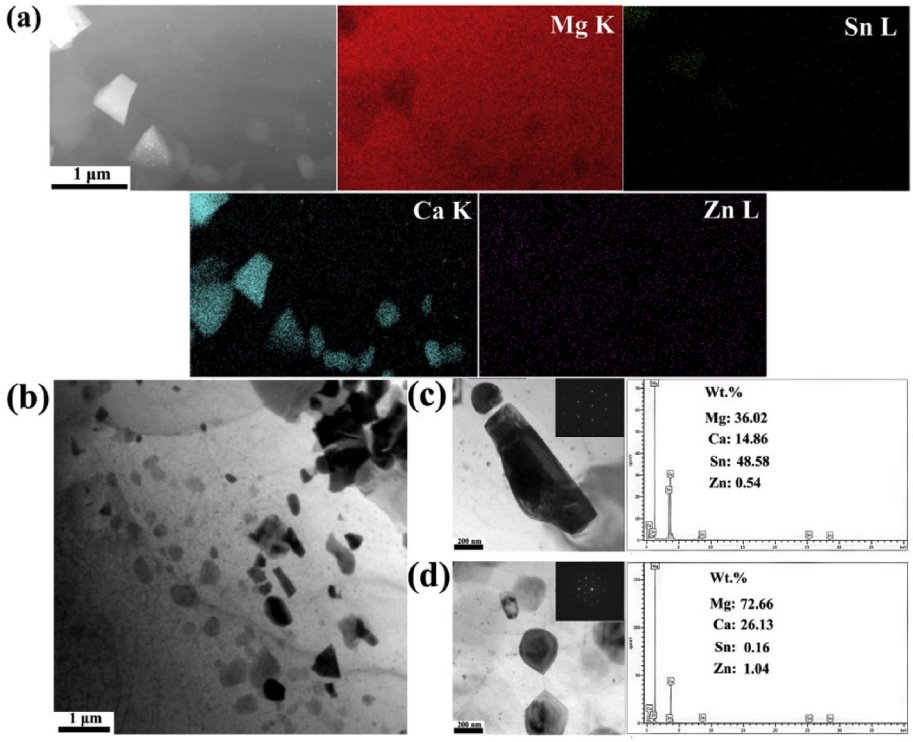

Fig. 5. (a) EDS mapping images of secondary phase particles in as-extruded Mg-1.0Sn-0.5Zn-2.0Ca alloy sheet. (b) Bright-field TEM micrograph. Typical precipitates along with their diffraction patterns by SAED and compositions by EDS: (c) CaMgSn precipitate phase; (d) Mg_2Ca precipitate phase.

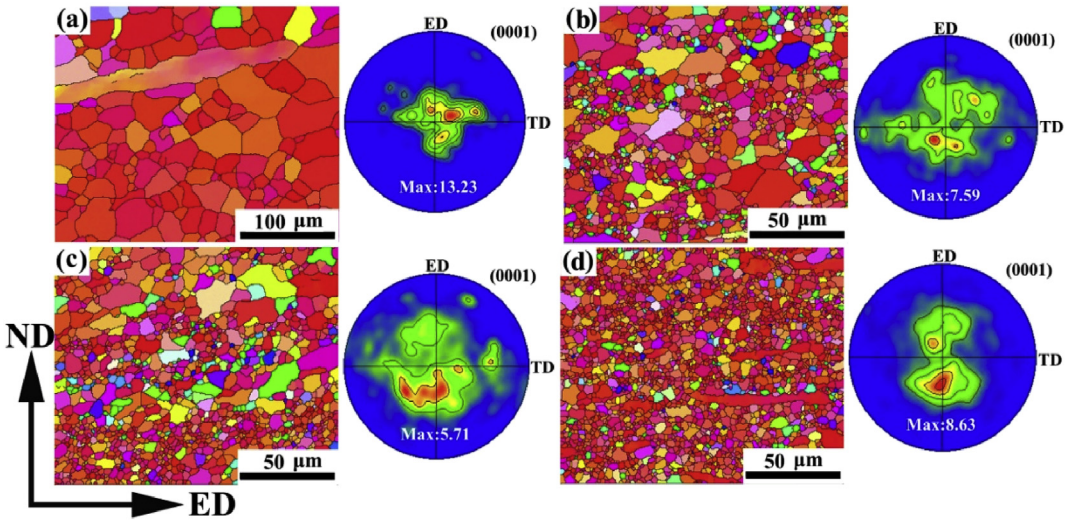

Fig. 6. EBSD inverse pole figure maps and (0001) pole figures from the ED-ND plane of as-extruded Mg-1.0Sn-0.5Zn-*x*Ca alloys: (a) 0.0 Ca alloy; (b) 0.5 Ca alloy; (c) 1.0 Ca alloy; (d) 2.0 Ca alloy.

grain refinement in the as-extruded Mg-1.0Sn-0.5Zn alloy. Such effect of Ca is consistent with the research of Wei [27], and possible reasons are ascribed to the synergistic effect of the following factors: (1) Grain size of the as-cast billets was significantly reduced via Ca addition. Previous research reported that an increase in the area of grain boundaries may provide more nucleation sites for DRX [28]. Hence, this reduced grain size of as-cast alloys would promote DRX during the extrusion process and then lead to grain refinement. (2) Fig. 9 summarizes the average grain size and volume fraction of secondary phase particles in as-extruded sheets as a function of Ca content. The amount of the secondary phase is directly proportional to the Ca content of Mg-Sn-Zn-Ca alloys and there is an inverse relationship between the average grain size and volume fraction of secondary phase. More intuitively, grains in the vicinity of secondary phase particles are much finer than those in the regions free of any particles (see Fig. 4). It implies that the thermally stable CaMgSn and Mg_2Ca precipitates can restrain the growth of DRXed grains during the extrusion process. Coincidentally, Kang et al. [29] also reported that Ca containing precipitates, which are mostly forming along the DRXed grain boundaries, could reduce the mobility of the grain boundaries and retard the grain growth during the extrusion process. (3) Ca atoms are easy to

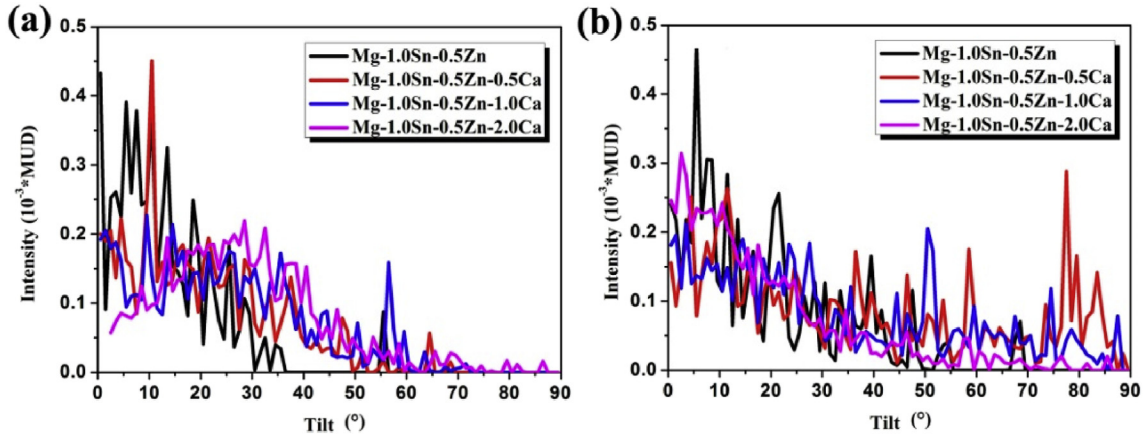

Fig. 7. Texture intensity in (0001) plane plotted as a function of tilt from the ND toward the ED (a) or TD (b), respectively.

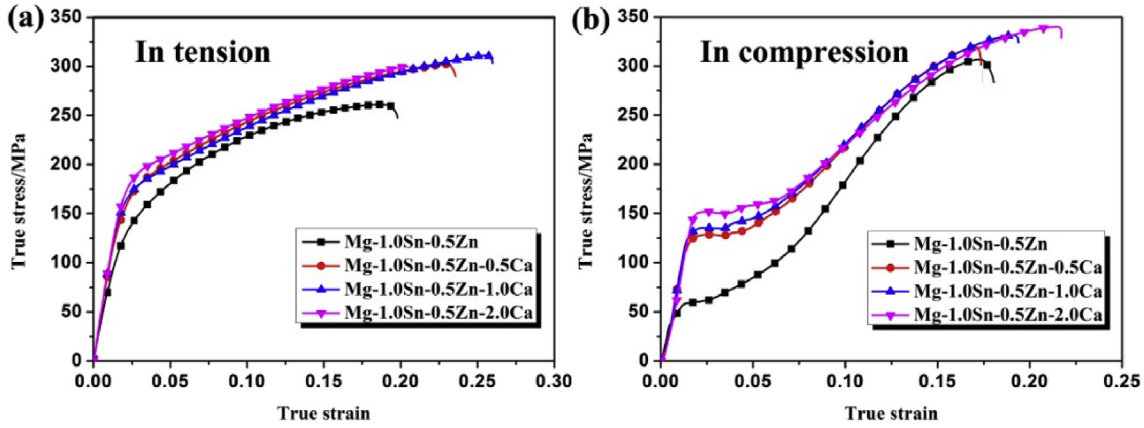

Fig. 8. The true tensile and compressive stress-strain curves of as-extruded Mg-1.0Sn-0.5Zn-based alloys.

Table 2
Summary of mechanical properties of four as-extruded alloys which suffer from uniaxial tensile and compressive tests along the ED.

Samples	In tension			In compression			CYS/TYS (ave.)
	TYS (MPa)	UTS (MPa)	EL (%)	CYS (MPa)	UCS (MPa)	EL (%)	
Mg-1.0Sn-0.5Zn-0.0Ca	134.9 ± 2.3	261.0 ± 2.7	17.4 ± 0.4	54.5 ± 1.3	310.5 ± 2.4	17.1 ± 0.3	0.40
Mg-1.0Sn-0.5Zn-0.5Ca	158.7 ± 1.9	302.2 ± 3.5	21.3 ± 0.3	114.5 ± 1.6	321.5 ± 3.5	16.0 ± 0.2	0.72
Mg-1.0Sn-0.5Zn-1.0Ca	167.3 ± 3.2	310.9 ± 3.7	23.6 ± 0.2	132.8 ± 2.1	331.3 ± 4.2	17.6 ± 0.2	0.79
Mg-1.0Sn-0.5Zn-2.0Ca	180.7 ± 2.7	300.0 ± 4.2	17.9 ± 0.1	151.1 ± 1.2	339.9 ± 2.7	19.6 ± 0.1	0.84

segregate at the grain boundaries [30] and the segregated Ca atoms may exert strong dragging force on the grain boundaries motion.

4.1.2. Texture

Fig. 10 presents the rare earth texture component of four as-extruded alloys. Distinguishing between the textural components of rare earth or the rest is based on the deviation of 20° between the ND and the c-axis of grain [31]. With Ca content rising from 0.0 to 0.5, 1.0 and 2.0 wt%, the percentage of rare earth texture component dramatically increased from ~62.5% to ~83.0–87.6%. Besides, as seen in Fig. 6, the microstructures of Ca-modified samples are obviously inhomogeneous and emerged plenty of fine equiaxed grains with an average grain size of 0.5–1.5 μm compared to those of Ca-free sample. Correspondingly, the correlation between grain size and texture of Mg-Sn-Zn-Ca alloys are also showed in Fig. 11, where total grains are divided into two parts depending on the grain size of 3 μm. The results manifest that both parts of the grains exhibit the ED-split texture and similar value of maximum pole intensity.

The possible reasons of a weakened ED-split texture in Ca-modified samples are pertaining to the solid solubility of Ca element [32] and the varied DRX behavior during the extrusion process [33] compared to that of Ca-free sample with typical basal texture. Previous research [34] indicated that the Ca element, which is similar to RE elements with a larger atom radius than that of Mg element, could weaken the basal texture when alloyed with Mg alloy. Ding et al. [35] also revealed that Ca solute addition gave rise to the decreased c/a ratio and stacking fault energy (SFE) of non-basal slips, which eventually led to the formation of ED-split textures of Ca-containing alloys. Another reason can be ascribed to the varied DRX behavior derived from secondary phase particles during the extrusion process. In general, DRX behavior consists of

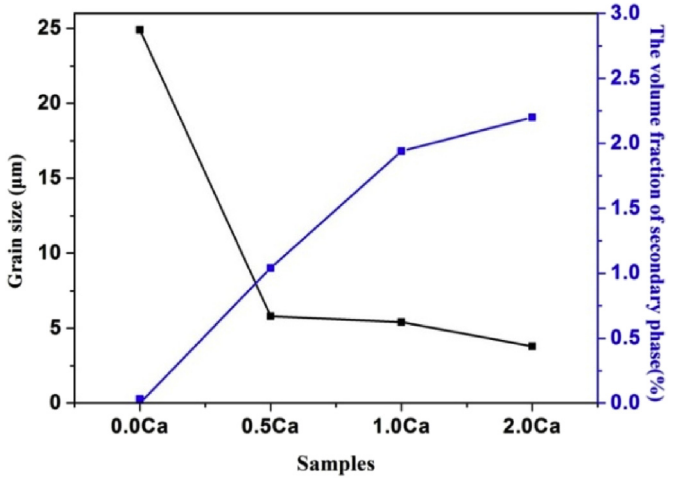

Fig. 9. The summary of average grain size and volume fraction of secondary phase for four as-extruded samples.

two processes: nucleation and growth. Hence, the effects of thermally stable CaMgSn and Mg_2Ca particles on DRXed nucleation and the DRXed grain growth should be analyzed. Fig. 12 presents the EBSD mappings of different types of grains, which show recrystallized regions (blue areas), sub-grains (yellow areas), deformed regions (red areas), their corresponding fraction and composed (0001) pole figures. The result reveals that Ca addition significantly decreases the recrystallized grain fraction of Mg-Sn-Zn alloy. Similarly, Du et al. [36] also expressed that the addition of 0.4 or 0.8 wt% Ca in the as-extruded Mg-6Zn alloy could postpone or inhibit DRX during the extrusion process. According to particle-stimulated nucleation (PSN) of recrystallization theory, particles can either promote or suppress DRX nucleation depending largely on their size. More detailed, large particles (>1 μm) could act as effective nucleation sites to accelerate DRX by increasing the dislocation density, whereas fine particles (<1 μm) could induce the grain-boundary pinning effect and eventually retard the DRX behavior [37,38]. In the present study, CaMgSn and Mg_2Ca particles with the size mainly fragmented into <1 μm during the extrusion process (see Fig. 4), are accounting for the phenomenon that

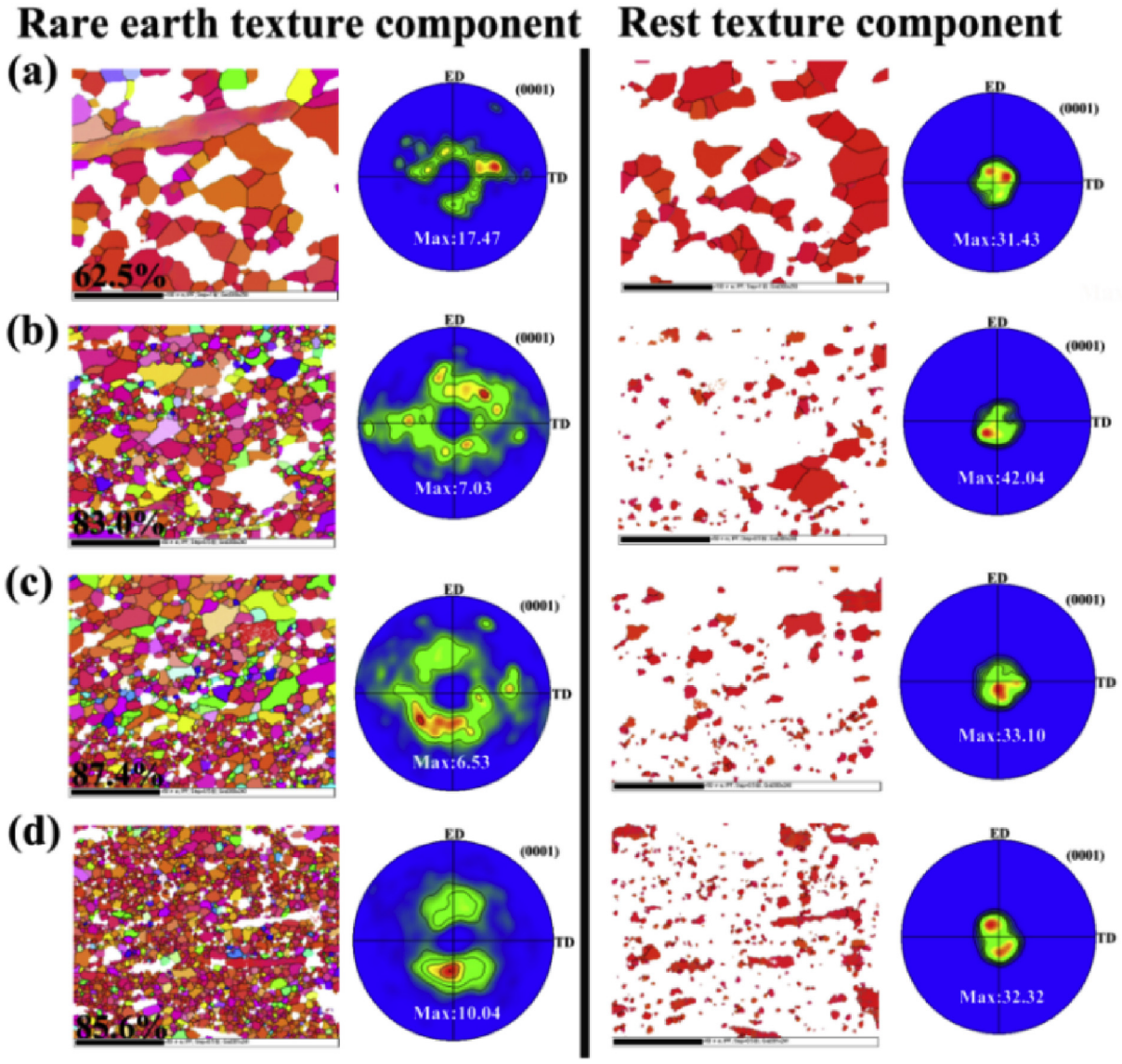

Fig. 10. Rare earth texture component of four as-extruded alloys: (a) Mg-1.0Sn-0.5Zn alloy. (b) Mg-1.0Sn-0.5Zn-0.5Ca alloy. (c) Mg-1.0Sn-0.5Zn-1.0Ca alloy. (d) Mg-1.0Sn-0.5Zn-2.0Ca alloy.

decreased DRXed fraction of Mg-Sn-Zn alloy via Ca addition. It is noteworthy that the distribution of DRXed grains in (0001) pole figures (see Fig. 12) via PSN mechanism are more disperse than that of substructured and deformed grains. Previous studies [39,40] also stated that DRXed grains via PSN mechanism possessed a relatively random orientation and contributed to the weakening of overall texture by making the orientation coherency with parent grains diminished rapidly. Additionally, the secondary phase particles may affect the preferential grain growth and result in the weakening of the recrystallization texture [41,42]. Coincidentally, Laser et al. [43] stated that the texture weakening of AZ31 alloys with 0.4 or 0.8 wt% Ca addition was pertaining to the grain boundary pinning effect originated from precipitated particles. As mentioned above, the enhanced possibility of non-basal slip activations via Ca solute atom and the varied DRX behavior derived from CaMgSn and Mg_2Ca particles jointly lead to the weakened ED-split texture of Ca-modified samples.

4.2. Effect of Ca addition on tensile properties

In general, yield strength of wrought magnesium alloys was closely associated with grain size, secondary phase particles and texture [44]. According to the Hall–Petch relationship [45], the grain boundary strengthening effect can be estimated as follows:

$$\sigma_y = \sigma_0 + kd^{-1/2} \quad (1)$$

Where σ_y is the yield strength, σ_0 is the frictional stress, k is the Hall–Petch coefficient and d is the average grain size. Evidently, the yield strength is inversely proportional to the grain size, and the fine grains serve to enhance the yield strength of the alloy. By assuming that all the as-extruded alloys in the present study have identical values of σ_0 and k, the increase in yield strength due to grain refinement via Ca addition can be expressed as follows:

$$\Delta\sigma = k\left(d^{-1/2}_{MgSnZn-x(0.5,1.0,2.0wt\%)Ca} - d^{-1/2}_{MgSnZn}\right) \quad (2)$$

The k value of the present as-extruded alloys is 170 MPa $\mu m^{-1/2}$ and the measured average grain size of these four as-extruded alloys is 24.9, 5.8, 5.4 and 3.8 μm, respectively. Hence, compared with the Mg-1.0Sn-0.5Zn alloy, the increments of yield strength for the Mg-1.0Sn-0.5Zn-x(0.5, 1.0, 2.0 wt%) Ca alloys causing by grain refinement are 36.5, 39.1 and 53.2 MPa, respectively. Secondary phase is another crucial parameter that strongly affects the yield strength of the alloy. Sun et al. [46] indicated that hard particles dispersed in a soft α-Mg matrix may block the movement of dislocation, cause dislocations pile-ups, and thus contributing to the strength improvement. Assuming that the CaMgSn and Mg_2Ca phase particles are not sheared by the dislocations, their strengthening mechanism follows the Orowan process. An increase in YS is depended on the uniform diameter (D) and volume fraction (f) of the secondary phase precipitates, which is according to the following equation:

$$YS \propto f^{1/2}D^{-1} \ln D \quad (3)$$

Apparently, increasing volume fraction of the secondary phase can improve the yield strength of the alloy. Correspondingly, in the present study, the increasing amount of secondary phase precipitates as Ca content increases (see Fig. 9) also contributes to the yield strength enhancement of Mg-Sn-Zn alloy. Fig. 13 depicts the distribution maps of Schmid Factor (SF) for basal slip of four as-extruded alloys in tension along the ED. The result reflects that Ca addition significantly increases the average SF for basal slip, which means the easier activation of basal slip [47]. Hence, ED-split

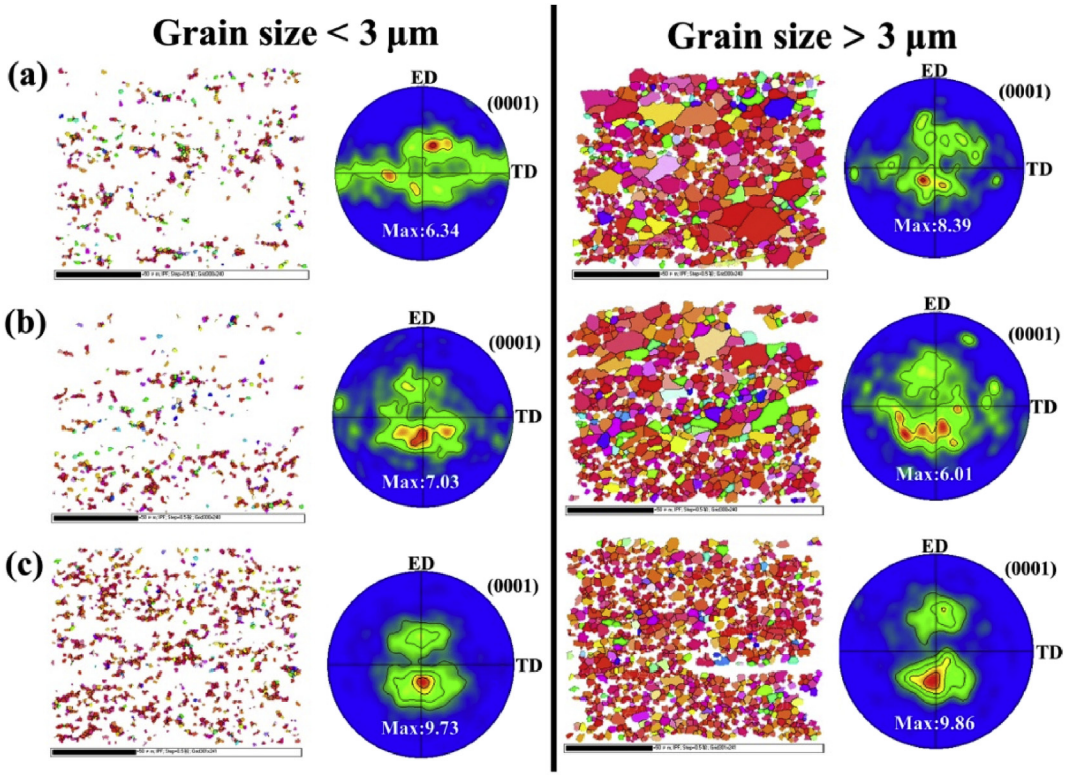

Fig. 11. EBSD IPF maps in the ED-ND plane and {0001} pole figures of three as-extruded Mg-Sn-Zn-Ca alloys corresponding to grains with size <3 μm and >3 μm, respectively. (a) Mg-1.0Sn-0.5Zn-0.5Ca alloy. (b) Mg-1.0Sn-0.5Zn-1.0Ca alloy. (c) Mg-1.0Sn-0.5Zn-2.0Ca alloy.

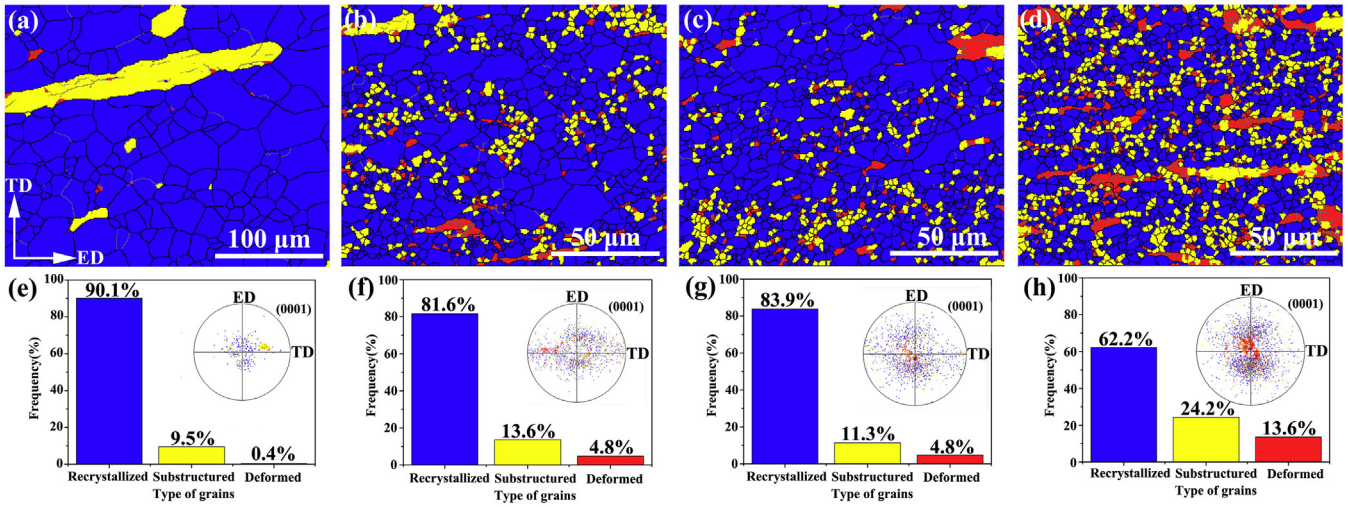

Fig. 12. Different types of grains of as-extruded (a) Mg-1.0Sn-0.5Zn alloy, (b) Mg-1.0Sn-0.5Zn-0.5Ca alloy, (c) Mg-1.0Sn-0.5Zn-1.0Ca alloy, (d) Mg-1.0Sn-0.5Zn-2.0Ca alloy: blue-recrystallized, yellow-substructured, red-deformed; (e), (f), (g) and (h) frequency and corresponding (0001) pole figures of the different types of grains shown in (a), (b), (c) and (d), respectively. (For interpretation of the references to colour in this figure legend, the reader is referred to the Web version of this article.)

texture provides a negligible contribution to the yield strength improvement of Mg-Sn-Zn-Ca alloys. As a result, it can be deduced that the improvement of YS for Ca-modified samples compared to Ca-free sample is ascribed to the strengthening effect induced by the grain refinement and CaMgSn and Mg_2Ca phase particles overwhelm the weakening effect of their ED-spilt texture.

Notably, among the four as-extruded alloys, Mg-1.0Sn-0.5Zn-1.0Ca alloy possesses the highest EL of 23.8% in tension, which is enhanced by about 6.4% than that of Mg-1.0Sn-0.5Zn alloy. The actual reasons can be summed up into the following two factors. Firstly, the addition of Ca results in noticeable grain refinement, which is beneficial to the dislocation slip and then leads to a higher strain coordination capability between grains during plastic deformation [48]. Secondly, all Ca-modified samples present the weakened ED-split texture compared to Ca-free sample with typically strong basal texture. A weakened ED-split texture would make more grains deviate far from the hard orientation [49] and facilitate the activation of basal slip in tension along the ED, which are consequently in favor of the ductility improvement. However, it can be found that the excess Ca addition (2.0 wt%) substantially deteriorated the ductile performance of alloy instead. The main reason was lying in that hard secondary phase particles in a metallic material often became the sites for stress concentration, void nucleation and then accelerated cracks eventually [50]. Therefore, Ca addition inducing the improvement of ductile is originated from the grain refinement and texture modification, whereas excessive Ca content gives rise to the increasing quantity of secondary phase particles (especially the Mg_2Ca phase), and it is more likely to counteract the positive effect of fine grains and weakened ED-split texture on their ductility.

4.3. Improved tension-compression yield asymmetry achieved by Ca addition

As shown in Table 2, the value of CYS/TYS of Mg-Sn-Zn-based alloys is significantly increased from 0.40 to 0.72–0.84 as the Ca content increases. Generally speaking, the significant tension-compression yield asymmetry (TCA) was originated from the

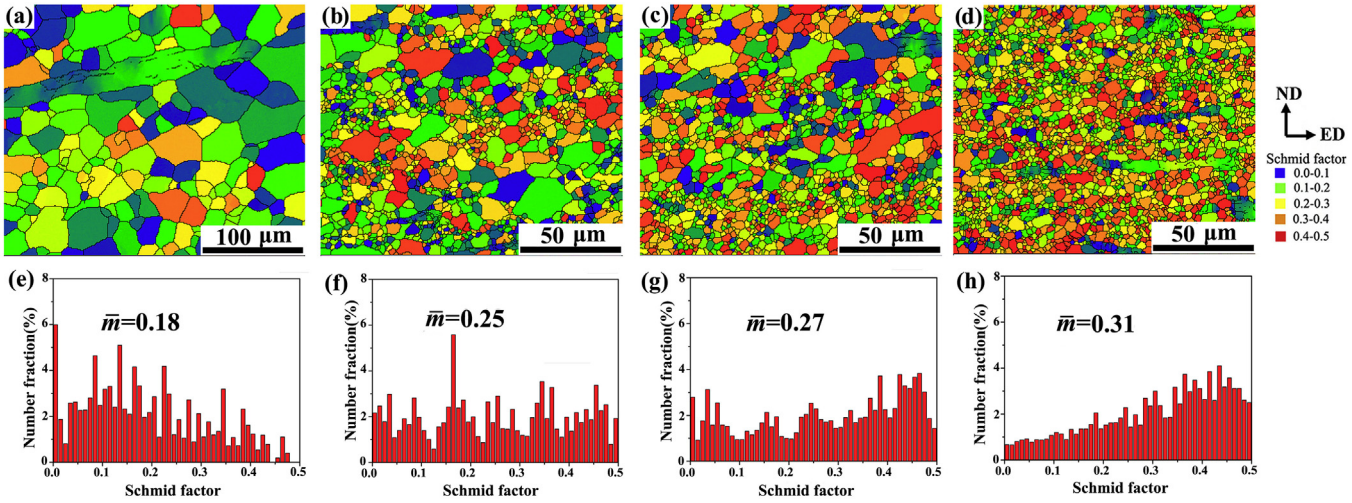

Fig. 13. The quantitative analysis of (0001)/<11–20> basal slip Schmid factor (SF) of the as-extruded alloys (when the tensile direction is parallel to extrusion direction): (a), (e) Mg-1.0Sn-0.5Zn alloy; (b), (f) Mg-1.0Sn-0.5Zn-0.5Ca alloy; (c), (g) Mg-1.0Sn-0.5Zn-1.0Ca alloy; (d), (h) Mg-1.0Sn-0.5Zn-2.0Ca alloy.

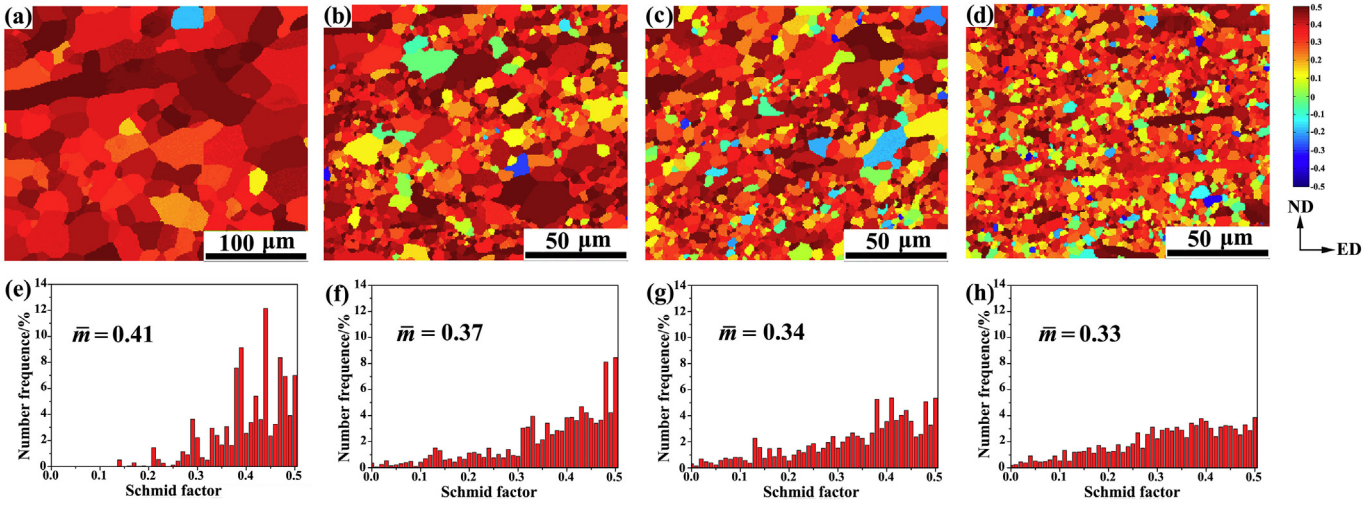

Fig. 14. Schmid factor as a function of relative spatial position and relative distributions for {10−12} twinning under compression along the ED: (a), (e) Mg-1.0Sn-0.5Zn alloy; (b), (f) Mg-1.0Sn-0.5Zn-0.5Ca alloy; (c), (g) Mg-1.0Sn-0.5Zn-1.0Ca alloy; (d), (h) Mg-1.0Sn-0.5Zn-2.0Ca alloy. Note that a negative value of SF for {10−12} twinning would lead to contraction along the C-axes of grains and not be activated. A minus SF for {10−12} twinning is therefore treated as zero during calculation of the distribution of SFs.

deformation twining polarity and the discrepancy of activated stress between deformation twinning and slip systems [51]. Furthermore, in association with the TCA, grain size and texture have generally been regarded as the main factors, because they cloud influence twinning under compression [52]. Dogan et al. [53] stated that grain size dependence of tensile twinning mode was considered to be more pronounced than that of dislocation slips. Hence, obviously decreased TCA of Ca-modified samples in the current work can be partly attributed to the twin suppressing induced by grain refinement. Furthermore, in order to reveal the contribution of texture modification caused by Ca addition to the TCA improvement, the average SF for {10−12} twins under compression along the ED is calculated with the results shown in Fig. 14. Apparently, there is a downward trend in the average SF for {10−12} twining as Ca content increases, which implies that twining under compression is relatively more difficult in the Ca-modified samples (i.e. weakened ED-split texture) than that in the Ca-free sample (i.e. typical strong basal texture). Additionally, the twins are susceptible to secondary phase particles, especially their distribution [54]. The particles, which were distributed inside grains, could offer resistance to the propagation and growth of twins, whereas the counterparts were merely distributed at the grain boundary cannot offer [55]. In the present study, both blocky CaMgSn particle (partly distributed within grain) and spherical Mg_2Ca particle (distributed as a cluster), which are considered to retard the nucleation, propagation and growth of twins, thus further reduce TCA [56,57]. As a result, owing to the grain refinement, texture modification and newly formed CaMgSn and Mg_2Ca phase particles, the TCA performance of as-extruded Mg-Sn-Zn alloy is significantly improved via Ca addition.

5. Conclusions

1. The addition of Ca to the as-cast Mg-1.0Sn-0.5Zn alloy resulted in grain refinement and microstructure variation from equiaxed-liked grains to typical dendrites, meanwhile secondary phase had transformed from Mg_2Sn to CaMgSn, Mg_2Ca and $Ca_2Mg_6Zn_3$ (in the minority).
2. As Ca content increased from 0.0 to 2.0 wt%, the grain size of as-extruded Mg-Sn-Zn alloy was significantly decreased from ~25 μm to 4–6 μm, whereas the texture type was converted from strong basal texture to weakened ED-split texture.
3. The improvement of tensile ductility via (0–1.0 wt%) Ca addition was originated from the grain refinement and texture modification, whereas excessive Ca content (2.0 wt%) deteriorated it instead. The main reason was that the increased quantity of Mg_2Ca phase particles would offset the contributions to ductility from fine grains and weakened ED-split texture. As-extruded Mg-1.0Sn-0.5Zn-2.0Ca alloy possessed the highest CYS (151.1 MPa) and TYS (180.7 MPa) among the Mg-Sn-Zn based alloys, which is primarily due to the most significant grain refinement and precipitation strengthening. Besides, improved TCA performance of Mg-Sn-Zn alloy via Ca addition can be ascribed to the combined effects of refined grains, weakened ED-split texture and newly formed CaMgSn and Mg_2Ca phase particles.

Acknowledgements

The authors are grateful for the financial supports from the National Key Research and Development Program of China, China (2016YFB0301104), and the National Natural Science Foundation of China, China (51531002 and U1764253), Chongqing Science and Technology Commission, China (cstc2014jcyjjq0041, cstc2014jcyjjq50002, cstc2015zdcy-ztzx50003 and cstc2015yykfc5001), and the Fundamental Research Funds the Central Universities, China (106112016CDJZR138801).

References

[1] T. Laser, C. Hartig, M.R. Nürnberg, D. Letzig, R. Bormann, The influence of calcium and cerium mischmetal on the microstructural evolution of Mg-3Al-1Zn during extrusion and resulting mechanical properties, Acta Mater. 56 (2008) 2791–2798.
[2] J. Xu, J.F. Song, B. Jiang, J.J. He, Q.H. Wang, B. Liu, G.S. Huang, F.S. Pan, Effect of effective strain gradient on texture and mechanical properties of Mg-3Al-1Zn alloy sheets produced by asymmetric extrusion, Mater. Sci. Eng. A 706 (2017) 172–180.
[3] Q.H. Wang, B. Jiang, A.T. Tang, S.X. Ma, Z.T. Jiang, Y.F. Chai, B. Liu, F.S. Pan, Ameliorating the mechanical properties of magnesium alloy: role of texture, Mater. Sci. Eng. A 689 (2017) 395–403.
[4] D. Liu, J.F. Song, B. Jiang, Y. Zeng, Q.H. Wang, Z.T. Jiang, B. Liu, G.S. Huang, F.S. Pan, Effect of Al content on microstructure and mechanical properties of as-cast Mg-5Nd alloys, J. Alloys Compd. 737 (2018) 263–270.
[5] Y.Z. Du, X.G. Qiao, M.Y. Zheng, K. Wu, S.W. Xu, The microstructure, texture and

mechanical properties of extruded Mg–5.3Zn–0.2Ca–0.5Ce (wt%) alloy, Mater. Sci. Eng. A 620 (2015) 164–171.
[6] Y. Zeng, O.L. Shi, B. Jiang, G.F. Quan, F.S. Pan, Improved formability with theoretical critical shear strength transforming in Mg alloys with Sn addition, J. Alloys Compd. 764 (2018) 555–564.
[7] C.Y. Zhao, X.H. Chen, F.S. Pan, S.Y. Gao, D. Zhao, X.F. Liu, Effect of Sn content on strain hardening behavior of as-extruded Mg-Sn alloys, Mater. Sci. Eng. A 713 (2018) 244–252.
[8] F. Wang, T. Hu, Y.T. Zhang, W.L. Xiao, C.L. Ma, Effects of Al and Zn contents on the microstructure and mechanical properties of Mg-Al-Zn-Ca magnesium alloys, Mater. Sci. Eng. A 704 (2017) 57–65.
[9] R.Q. Zhang, J.F. Wang, S. Huang, S.J. Liu, F.S. Pan, Substitution of Ni for Zn on microstructure and mechanical properties of Mg–Gd–Y–Zn–Mn alloy, J. Magn. Alloys 5 (2017) 355–361.
[10] C.L. Mendis, C.J. Bettles, M.A. Gibson, C.R. Hutchinson, An enhanced age hardening response in Mg–Sn based alloys containing Zn, Mater. Sci. Eng. A 435 (2006) 163–171.
[11] T.T. Sasaki, K. Ohishi, T. Ohkubo, K. Hono, Enhanced age hardening response by the addition of Zn in Mg–Sn alloys, Scripta Mater. 55 (2006) 251–254.
[12] C.Q. Liu, H.W. Chen, J.F. Nie, Interphase boundary segregation of Zn in Mg–Sn–Zn alloys, Scripta Mater. 123 (2016) 5–8.
[13] Y.M. Kim, C.D. Yim, H.S. Kim, B.S. You, Key factor influencing the ignition resistance of magnesium alloys at elevated temperatures, Scripta Mater. 65 (2011) 958–961.
[14] Z.T. Jiang, B. Jiang, H. Yang, Q.H. Wang, J.H. Dai, F.S. Pan, Influence of the Al2Ca phase on microstructure and mechanical properties of Mg–Al–Ca alloys, J. Alloys Compd. 647 (2015) 357–363.
[15] Y.F. Chai, B. Jiang, J.F. Song, Q.H. Wang, J.J. He, J. Zhao, G.S. Huang, Z.T. Jiang, F.S. Pan, Role of Al content on the microstructure, texture and mechanical properties of Mg-3.5Ca based alloys, Mater. Sci. Eng. A 730 (2018) 303–316.
[16] H.C. Pan, G.W. Qin, M. Xu, H. Fu, Y.P. Ren, F.S. Pan, Z.Y. Gao, C.Y. Zhao, Q.S. Yang, J. She, B. Song, Enhancing mechanical properties of Mg-Sn alloys by combining addition of Ca and Zn, Mater. Des. 83 (2015) 736–744.
[17] H.C. Pan, G.W. Qin, Y.M. Huang, Y.P. Ren, X.C. Sha, X.D. Han, Z.Q. Liu, C.F. Li, X.L. Wu, H.W. Chen, C. He, L.J. Chai, Y.Z. Wang, J.F. Nie, Development of low-alloyed and rare-earth-free magnesium alloys having ultra-high strength, Acta Mater. 149 (2018) 350–363.
[18] G. Nayyeri, R. Mahmudi, Effects of Ca additions on the microstructural stability and mechanical properties of Mg–5%Sn alloy, Mater. Des. 32 (2011) 1571–1576.
[19] G.H. Hasani, R. Mahmudi, Tensile properties of hot rolled Mg–3Sn–1Ca alloy sheets at elevated temperatures, Mater. Des. 32 (2011) 3736–3741.
[20] S. Farahany, H.R. Bakhsheshi-Rad, M.H. Idris, M.R. Abdul Kadir, A.F. Lotfabadi, A. Ourdjini, In-situ thermal analysis and macroscopical characterization of Mg–xCa and Mg–0.5Ca–xZn alloy systems, Thermochim. Acta 527 (2012) 180–189.
[21] P.M. Jardim, G. Solorzano, J.B. Vander Sande, Second phase formation in melt-spun Mg–Ca–Zn alloys, Mater. Sci. Eng. A 381 (2014) 196–205.
[22] Y. Chino, X. Huang, K. Suzuki, K. Sassa, M. Mabuchi, Influence of Zn concentration on stretch formability at room temperature of Mg-Zn-Ce alloy, Mater. Sci. Eng. A 528 (2010) 566–572.
[23] Y. Ali, D. Qiu, B. Jiang, F.S. Pan, M.X. Zhang, Current research progress in grain refinement of cast magnesium alloys: a review article, J. Alloys Compd. 619 (2015) 639–651.
[24] B. Jiang, Y. Zeng, M.X. Zhang, H.M. Yin, Q.S. Yang, F.S. Pan, Effects of Sn on microstructure of as-cast and as-extruded Mg–9Li alloys, Trans. Nonferrous Metals Soc. China 23 (2013) 904–908.
[25] Z.T. Jiang, B. Jiang, J.Y. Zhang, X.S. Xia, F.S. Pan, Microstructural evolution of Mg-4Al-2.5Ca alloy during solidification, Mater. Sci. Forum 816 (2015) 486–491.
[26] X.D. Peng, J.C. Li, S.Y. Xie, G.B. Xie, Y. Yang, Effects of different state Mg-5Sr-10Y master alloys on the microstructure refinement of AZ31 magnesium alloy, Rare Metal Mater. Eng. 42 (2013) 2421–2426.
[27] J.Y. Wei, J.H. Chen, H.G. Yan, B. Su, X.Q. Pan, Effects of minor Ca addition on microstructure and mechanical properties of the Mg-4.5 Zn-4.5 Sn-2Al-based alloy system, J. Alloys Compd. 548 (2013) 52–59.
[28] C.D. Barrett, A. Imandoust, A.L. Oppedal, K. Inal, M.A. Tschopp, H. El Kadiri, Effect of grain boundaries on texture formation during dynamic recrystallization of magnesium alloys, Acta Mater. 128 (2017) 270–283.
[29] Q. Kang, H.T. Jiang, Y. Zhang, Z. Xu, H. Li, Z.H. Xia, Effect of various Ca content on microstructure and fracture toughness of extruded Mg-2Zn alloys, J. Alloys Compd. 742 (2018) 1019–1030.
[30] Z.R. Zeng, Y.M. Zhu, S.W. Xu, M.Z. Bian, C.H.J. Davies, N. Birbilis, J.F. Nie, Texture evolution during static recrystallization of cold-rolled magnesium alloys, Acta Mater. 105 (2016) 479–494.
[31] G.G. Wang, G.S. Huang, X. Chen, Q.Y. Deng, A.T. Tang, B. Jiang, F.S. Pan, Effects of Zn addition on the mechanical properties and texture of extruded Mg-Zn-Ca-Ce magnesium alloy sheets, Mater. Sci. Eng. A 705 (2017) 46–54.
[32] N. Stanford, Micro-alloying Mg with Y, Ce, Gd and La for texture modification—a comparative study, Mater. Sci. Eng. A 527 (2010) 10–11.
[33] S.H. Kim, J.U. Lee, Y.J. Kim, J.G. Jung, S.H. Park, Controlling the microstructure and improving the tensile properties of extruded Mg-Sn-Zn alloy through Al addition, J. Alloys Compd. 751 (2018) 1–11.
[34] N. Stanford, The effect of calcium on the texture, microstructure and mechanical properties of extruded Mg–Mn–Ca alloys, Mater. Sci. Eng. A 528 (2010) 314–322.
[35] H.L. Ding, X.B. Shi, Y.Q. Wang, G.P. Cheng, S. kamado, Texture weakening and ductility variation of Mg–2Zn alloy with CA or RE addition, Mater. Sci. Eng. A 645 (2015) 196–204.
[36] Y.Z. Du, X.G. Qiao, M.Y. Zheng, D.B. Wang, K. Wu, I.S. Golovin, Effect of microalloying with Ca on the microstructure and mechanical properties of Mg-6 mass%Zn alloys, Mater. Des. 98 (2016) 285–293.
[37] S.H. Park, J.G. Jung, Y.M. Kim, B.S. You, A new high-strength extruded Mg-8Al-4Sn-2Zn alloy, Mater. Lett. 139 (2015) 35–38.
[38] J.D. Robson, D.T. Henry, B. Davis, Particle effects on recrystallization in magnesium–manganese alloys: particle-stimulated nucleation, Acta Mater. 57 (2009) 2739–2747.
[39] M. Yuasa, N. Miyazawa, M. Hayashi, M. Mabuchi, Y. Chino, Effects of group II elements on the cold stretch formability of Mg–Zn alloys, Acta Mater. 83 (2015) 294–303.
[40] Y. Chino, X.S. Huang, K. Suzuki, M. Mabuchi, Enhancement of stretch formability at room temperature by addition of Ca in Mg-Zn alloy, Mater. Trans. 51 (2010) 818–821.
[41] C.F. Fang, Z.H. Wen, X.T. Liu, H. Hao, G.Q. Chen, X.G. Zhang, Microstructures and mechanical properties of Mg2Sn-nanophase reinforced Mg–Mg2Sn composite, Mater. Sci. Eng. A 684 (2017) 229–232.
[42] A. Imandoust, C.D. Barrett, A.L. Oppedal, W.R. Whittington, Y. Paudel, H.E. Kadiri, Nucleation and preferential growth mechanism of recrystallization texture in high purity binary magnesium-rare earth alloys, Acta Mater. 138 (2017) 27–41.
[43] T. Laser, C. Hartig, M.R. Nürnberg, D. Letzig, R. Bormann, The influence of calcium and cerium mischmetal on the microstructural evolution of Mg–3Al–1Zn during extrusion and resulting mechanical properties, Acta Mater. 56 (2008) 2791–2798.
[44] L.B. Tong, M.Y. Zheng, S. Kamado, D.P. Zhang, J. Meng, L.R. Cheng, H.J. Zhang, Reducing the tension–compression yield asymmetry of extruded Mg–Zn–Ca alloy via equal channel angular pressing, J. Magn. Alloys 3 (2015) 302–308.
[45] L. Zhang, M. Gong, L.M. Peng, Microstructure and strengthening mechanism of a thermomechanically treated Mg-10Gd-3Y-1SN-0.5Zr alloy, Mater. Sci. Eng. A 565 (2013) 262–268.
[46] H.F. Sun, C.J. Li, W.B. Fang, Evolution of microstructure and mechanical properties of Mg-3.0Zn-0.2Ca-0.5Y alloy by extrusion at various temperatures, J. Mater. Process. Technol. 229 (2016) 633–640.
[47] J. Bohlen, M.R. Nürnberg, J.W. Senn, D. Letzig, S.R. Agnew, The texture and anisotropy of magnesium–zinc–rare earth alloy sheets, Acta Mater. 55 (2007) 2101–2112.
[48] J. Koike, T. Kobayashi, T. Mukai, H. Watanabe, M. Suzuki, K. Maruyama, K. Higashi, The activity of non-basal slip systems and dynamic recovery at room temperature in fine-grained AZ31B magnesium alloys, Acta Mater. 51 (2003) 2055–2065.
[49] H.X. Wang, L.X. Zhang, W.Z. Chen, D.Q. Fang, W.C. Zhang, G.R. Gui, Improved tension/compression asymmetry achieved in high-strength magnesium alloys via compression-extrusion process, Mater. Sci. Eng. A 736 (2018) 239–247.
[50] J. Luo, H. Yan, N. Zheng, R.S. Chen, Effects of zinc and calcium concentration on the microstructure and mechanical properties of hot-rolled Mg-Zn-Ca sheets, Acta Metal. Sin. (Engl. Lett.) 29 (2016) 205–216.
[51] D.L. Yin, J.T. Wang, J.Q. Liu, X. Zhao, On tension-compression yield asymmetry in an extruded Mg–3Al–1Zn alloy, J. Alloys Compd. 478 (2009) 789–795.
[52] M.R. Barnett, A rationale for the strong dependence of mechanical twinning on grain size, Scripta Mater. 59 (2008) 696–698.
[53] E. Dogan, I. Karaman, G. Ayoub, G. Kridli, Reduction in tension–compression asymmetry via grain refinement and texture design in Mg–3Al–1Zn sheets, Mater. Sci. Eng. A 610 (2014) 220–227.
[54] J.D. Robson, N. Stanford, M.R. Barnett, Effect of particles in promoting twin nucleation in a Mg–5 wt.% Zn alloy, Scripta Mater. 63 (2010) 823–826.
[55] Y. Jiang, Y.A. Chen, J.J. Gao, Comparative study regarding the effect of Al, Zn, and Gd on the microstructure and mechanical properties of Mg alloy Mg-Sn-Li, Mater. Des. 105 (2016) 34–40.
[56] P.D. Wu, X.Q. Guo, H. Qiao, D.J. Lloyd, A constitutive model of twin nucleation, propagation and growth in magnesium crystals, Mater. Sci. Eng. A 625 (2015) 140–145.
[57] S. Kamrani, C. Fleck, Effects of calcium and rare-earth elements on the microstructure and tension–compression yield asymmetry of ZEK100 alloy, Mater. Sci. Eng. A 618 (2014) 238–243.